The Journal of Engineering Geology, Vol.7, No.1, April, 1997, pp.63-79

Discrimination of Local Microearthquakes and Artificial Underground Explosions on the Basis of Time-Frequency Domain
시간-주파수 영역에서의 국지 미소지진과 지하인공폭발의 구별

김 소 구 (Kim, So Gu) 한양대학교 지진연구소
박 용 철 (Park, Yong Cheol) 한양대학교 지진연구소

요약 / ABSTRACT

본 연구의 목적은 시간-주파수 영역에서의 미소지진과 인공폭발을 구별하는 것으로 미소지진과 인공폭발의 주파수특성을 연구하기 위해서 3차원 스펙트로그램(주파수, 시간, 진폭)을 이용하였다. 3차원 스펙트로그램은 국지 및 광역 거리에서 관측된 자료에 대하여 각각의 위상에 대한 주파수대역의 연구에 매우 유용한 방법이다. 채석장 발파로부터 관측된 P파와 S파는 10Hz 이상에서 큰 진폭을 가졌고 또한 가까운 거리에서는 뚜렷한 Rg파가 관측되었다. 미소 지진의 경우 P파와 S파는 넓은 주파수 대역에서 큰 진폭이 나타났다. 인공 폭발과 미소지진의 구별을 위해서는 10Hz 이하에서 Pg/Lg 스펙트럼 비를 이용하였고 각각의 위상에서의 정확한 시간창(time window)을 구하기 위해서 다중 필터 방법(MFM)을 이용하여 군속도를 계산하였다. 또한 3 성분 자료에 관해서는 자료의 순수한 P, SV, SH 성질을 구하기 위해 자유 표면에서의 영향을 보정하고 각각의 위상에 대하여 FFT을 실시하여 7개의 주파수 대역(0.5-3, 2-4, 3-5, 4-6, 5-7, 6-8, 8-10Hz)에서 Pg/Lg 스펙트럼 비를 계산하였다. 위의 과정을 통해 6-8Hz 대역에서 미소지진과 인공폭발이 가장 잘 구별되었다.

In this study, our purpose is to develop a technique to discriminate artificial explosions from local microearthquakes on the basis of time-frequency domain. To obtain spectral features of artificial explosions and microearthquakes, we used 3-d spectrograms(frequency, time and amplitude) because this is a useful tool to study the frequency content of entire seismic waveforms observed at local and regional distances (e. g., Kim et al., 1994). P and S waves from quarry blasts show that frequency content of dominant amplitude appeared above 10 Hz and Rg phases that are observed at near distance ranges. But P and S waves from microearthquakes have more broad frequency content as well as below 10 Hz. And for discrimination, Pg/Lg spectral ratio is performed below 10 Hz. In order to select

time windows we computed group velocity using multiple filter method(MFM) and removed free surface effects from all 3-components data for improving on data quality. Next step, we computed Fast-Fourier transform, and a log average spectral amplitude over seven frequency bands : 0.5 to 3, 2 to 4, 3 to 5, 4 to 6, 5 to 7, 6 to 8 and 8 to 10 Hz. The best separation is observed from 6 to 8 Hz.

Introduction

A growing interest, in discriminating explosions from earthquakes at local and/or regional distances, is associated with negotiations on a Comprehensive Test Ban Treaty (CTBT) as well as identifying(looking for) local active faults. The CTBT will call for a monitoring seismic network of international monitoring system(IMS) as well as local and/or regional monitoring to detect man-made seismic activities, such as quarry and mine blasts that often consist of several delayed blasts, sometimes referred to as "ripple firing" including clandestine underground explosions. If two or more explosions are fired at nearly same location but with small time delays, the seismically recorded waveforms for each of the explosions should be very similar although their amplitudes may vary if the sizes of delayed explosions are different. The amplitude spectrum computed on a time window which incorporates all the delayed-explosion signals will exhibit a characteristic modulation or scalloping pattern (Douglas and Kathleen, 1988). These ripple- fired chemical explosions may produce a unique spectral signature and recognition of these features facilitate discrimination of chemical from nuclear explosions and microearthquakes.

This study presented the concept of spectral modulations and spectral features of explosions and microearthquakes. And we also tried to discriminate using Pg/Lg spectral amplitude ratio over seven frequency bands.

Data Analysis

The data used for this study were recorded by temporal SIHY seismic array, BHS, SMW, KIGAM seismic array, IRIS(Inchon station) and KSRS seismic array. BHS and SMW stations are operated by SIHY in North of Seoul. BHS and temporal SIHY seismic array are equipped with velocity seismometers which are Springnether S-6000 and Mark Product L4C-3D respectively. KIGAM seismic array is equipped with 3 component seismometers either Markrand JV-100 or JV-200. JV-100 has 1 Hz natural frequency and its amplitude instrument response is flat to velocity from 1 to 12.5(50 SPS) or 25.5 (100 SPS), and JV-200 is broadband seismometer. IRIS Inchon station is a broadband type of seismometers(VBB, LP, VLP, ULP, VSP,...) but IRIS data used in this study are only two types, one is VBB(very broadband seismometer) whose sampling rate is 20 SPS on 24-bit channels from STS-1 seismomters, the other is VSP(very short period seismometer) whose sampling rate is 80 SPS and also 24-bit channels from 3 component STS-2 high gain seismometer. IRIS stations and KSRS seismic arrays have 8Hz cut off frequency(High cut filter). Thus we performed instrument correction that is divid amplitude spectrum into spectrum amplitude instrument slop in the frequency domain up to 10 Hz.

Table 1 shows configurations of each seismic stations.

Table 2 shows data of seismic events used in this study. Our data set of 23 small events(Md $\leq$ 4), of which 10 are explosions(event nos. 1 to 10) and 13 are micro earthquakes(event nos. 11 to 23). The hypocentral parameters of all explosion data are immediately determined on

previous studies(Kim et al., 1995; Kim and Park, 1996). And the events of number 23 and 24 are unknown events recorded at BHS on October, 31 1996 and December, 25 1996, respectively. Figure 1 shows location of events and each seismic stations. In this figure, open stars and dark stars present explosions and microearthquakes, respectively and crosses present unknown events. And closed triangles indicate KIGAM seismic array, open triangles and squares indicate SIHY temporal seismic stations and open circle indicates IRIS(Inchon) station and KSRS

Table 1. Configuration of seismic station.

Station Name	Latitude(°N)	Longitude(°E)	Place
BHS	37.65	126.96	Bukhan-san
SMW	37.75	127.16	Soomok-won
BBK	35.58	129.44	Bangbang-kol
CHS	36.18	129.09	
DKJ	35.94	129.11	Dukjung-ri
HAK	35.93	129.50	Hakge-ri
KJM	34.83	128.59	
SKMH	35.18	128.93	
MAK	35.37	129.18	Makok-ri
MKL	35.72	129.24	Myunke-ri
KSRS	37.48	127.90	Wonju
IRIS	37.48	126.63	Inchon
04/25/96*			
SIHY1-1	37.58	128.28	Kudu-mi
SIHY2-3	37.49	128.00	Hoengsung-gun
SIHY3-3	37.58	128.54	Mapyung-ri
04/26/96*			
SIHY1-1	37.50	127.63	Yongmun-san
SIHY2-3	37.50	128.07	Yongdun-ri
SIHY3-3	37.53	127.83	Sungji-bong

* Date of seismic experiment for studying of velocity structure in Central Korean Peninsula.

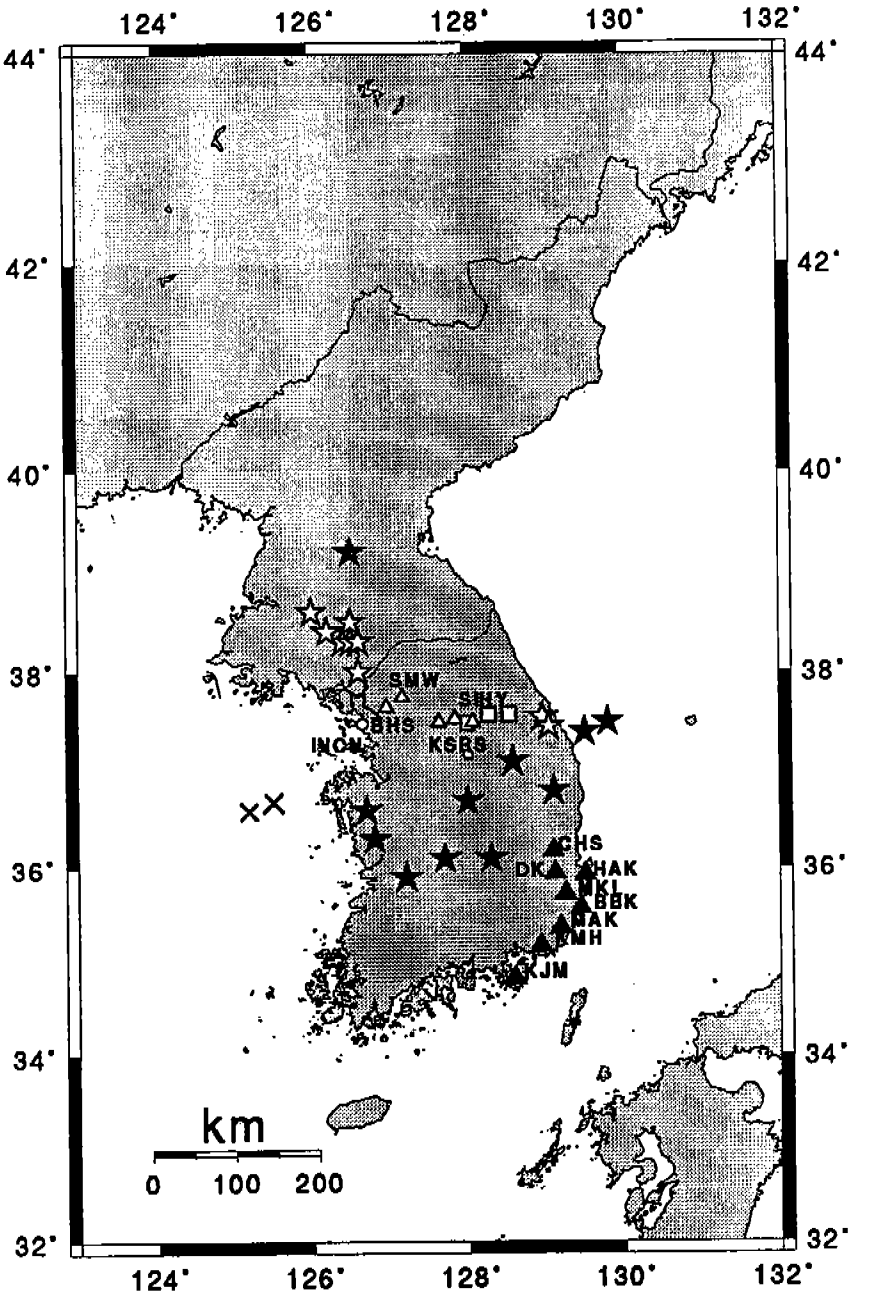

Figure 1. Locations of SIHY temporal seismic stations in the central Korean Peninsula (open square : 04/25/96 and open triangle : 04/26/96), KIGAM seismic station at Kyongsang basin, KSRS at wonju and IRIS station at Inchon(open circles). And open stars are explosions, dark stars are microearthquakes and cross is unknown datum.

Table 2. Explosoins and earthquakes used in this study.

No.	Event	Date	O. T.	Station	Epi.	Lat.	Long.	Mag.	SPS**
		M/D/Y	H : M : S		km	°N	°E		
1	KSRS05	01/17/88	12 : 25 : 25.3	KSRS	150.1	38.3	126.4	2.1	20
2	KSRS07	01/19/88	16 : 13 : 28.0	KSRS	181.0	38.4	126.2	2.4	20
3	KSRS09	01/24/88	13 : 14 : 28.8	KSRS	147.9	38.3	126.5	2.7	20
4	KSRS15B	01/28/88	16 : 59 : 02.1	KSRS	134.0	38.3	126.6	2.4	20
5	KSRS21	01/29/88	17 : 00 : 35.3	KSRS	206.0	38.6	126.0	2.6	20
6	KSRS27	02/03/88	11 : 57 : 16.8	KSRS	130.7	38.0	126.6	2.6	20
7	KSRS29	02/03/88	16 : 18 : 45.8	KSRS	161.0	38.5	126.5	2.5	20
8	EXP1	04/25/96	16 : 50 : 21.9	SIHY1-1	61.5	37.5	128.9	3.0	100
				SIHY2-3	83.97				100
				SIHY3-3	37.49				100
9	EXP2	04/26/96	16 : 31 : 20.04	SIHY1-1	124.28	37.5	129.0	2.7	100
				SIHY2-3	85.25				100
				SIHY3-3	106.43				100
10	EXP3		16 : 32 : 13.46	SIHY1-1	124.28	37.5	129.0	2.7	100
				SIHY2-3	85.25				100
				SIHY3-3	106.43				100
11	Honsung	02/07/79	23 : 52 : 17.6	KSRS	140.0	36.6	126.7	3.5	20
12	Honsung	03/12/97	02 : 09 : 26.9	KSRS	140.0	36.6	126.7	4.0	20
13	Samchok	10/06/95	21 : 07 : 33.3	IRIS	221.3	37.5	129.8	3.7	20
14	Puyo	09/17/95	00 : 13 : 47.3	IRIS	130.9	36.3	126.8	2.4	80
15	Dukyu	04/13/96	20 : 21 : 12.6	IRIS	175.1	36.1	127.7	3.2	80
16	Kumi	10/16/96	04 : 45 : 58.8	BHS	209.1	36.1	128.3	3.3	100
17	Tongo-san	06/04/96	18 : 33 : 21.7	HAK	103.18	36.7	128.8	2.2	50
				MKL	113.53				50
				BBK	135.36				50
18	Ik-san	06/21/96	01 : 04 : 09.9	KJM	171.2	35.9	127.2	2.8	50
				DKJ	171.9				50
				CHS	172.81				50
				MKL	184.5				50
				MAK	187.0				50
				HAK	207.0				50
19	Samchok	08/03/96	00 : 06 : 59.3	CHS	129.09	37.3	129.3	2.8	50
				DKJ	155.53				50
				MKL	178.27				50
				MAK	218.81				100
20	Munkyong	08/14/96	18 : 10 : 03.8	CHS	98.56	36.6	128.1	2.7	50
				MKL	138.44				50
				MAK	164.69				100
				KMH	171.36				100
				KJM	197.77				100
21	Young-wol	12/14/96	17 : 20 : 29.35*	SMW	128.11	37.3	128.5	2.0	100
22	Unknown	10/31/96	13 : 58 : 37.8	BHS	179.8	36.7	125.3	3.3	100
23	Unknown	12/25/96	15 : 21 : 08.16	BHS	151.0	36.8	125.8	2.0	100

* no time correction

** Sampling per second

array(Wonju). Figures 2 and 3 show vertical seismograms of explosions and microearthquakes used in this study, respectively.

In order to study the spectral characteristics of explosions and microearthquakes, we computed frequency-time displays of seismograms (spectrogram). This method is a useful tool to study the frequency content of entire seismic waveforms observed at local and regional distances (e. g., Kim et al., 1994). In this computation, spectral estimates were calculated for each time moving window (usually use about 4 sec) with 75 per cent overlapping between each successive time window by applying the adaptive multi-taper spectral estimation method. Next, spectral estimates of all time windows were presented in time-frequency space using a continuous curvature surface gridding algorithm. All spectrograms shown in this study correspond to the signal velocity spectra.

We analysed three quarry blasts recorded on the SIHY temporal seismic stations during April 24 to 27, 1996. The first explosion is observed on April 25, 1996. The dynamites are loaded into 80 drill holes with 7.5 cm diameter (vertical 57, horizontal 23; event number 8) in depth 25m and total yield is 7,500 kg. On April 26, 1996, the second and third explosions are carried out in the all horizontal holes (8.0-cm-diameter drill hole and depth 8m) and total yield is 2,790 kg and 2,629 kg, respectively(event number 9 and 10 in the table 2). All of explosions have 100 msec delay tmie. Figure 4 shows spectrograms of quarry blasts and figure 5 and 6 show spectrograms of microearthquakes. Douglas and Kathleen(1988) consider the theoretically expected spectra of seismic signals from ripple-fired explosions, both single and multiple delays. They expressed the equation of multiple signal $y(t)$ with N delays, with Nth delay being scaled by α_N(a real value) and delayed by τ_N as :

$$y(t) = x(t) + \alpha_1 x(t-\tau_1) + \alpha_2 x(t-\tau_2) + \cdots + \alpha_N x(t-\tau_N) \quad (1)$$

The Fourier transforms is

$$Y(w) = X(w)(1 + \alpha_1 e^{-jw\tau_1} + \alpha_2 e^{-jw\tau_2} + \cdots + \alpha_N e^{-jw\tau_N}) \quad (2)$$

and the log power spectrum is expressed by

$$Log\,|\,Y(w)\,|^2 = Log[\,|\,x(w)\,|^2(1+\beta)] + Log(1-\frac{2}{1+\beta})[\sum_{n=1}^{N}(\alpha_n \cos w\tau_n + \sum_{m=n+1}^{N}\alpha_n\alpha_m \cos w(\tau_n-\tau_m))] \quad (3)$$

where $\beta = \sum_{n=1}^{N}\alpha_n^2$ is constant in τ.

They analyze the above equation in the cepstrum and this equation shows the various periodicities in the spectral modulations depend not only on the basic delay, τ_n, but also on the interaction of delays, $\tau_n - \tau_m$. The required coarseness[1] of the fragmentation governs the length of the delays, with longer delays required for higher coarseness. For ground-vibration reduction, the required delay interval is directly proportional to the period of the strongest vibrations (Chapman et al.; Douglas and Kathleen, 1988). Smith(1989) also examined the effect of ripple firing on a sequence of shots at a single location. He used u(t) as the seismic signal from a single shot and U(f) as its Fourier

1) diameter(phi) of the fragmentation that is caused by exlosion.

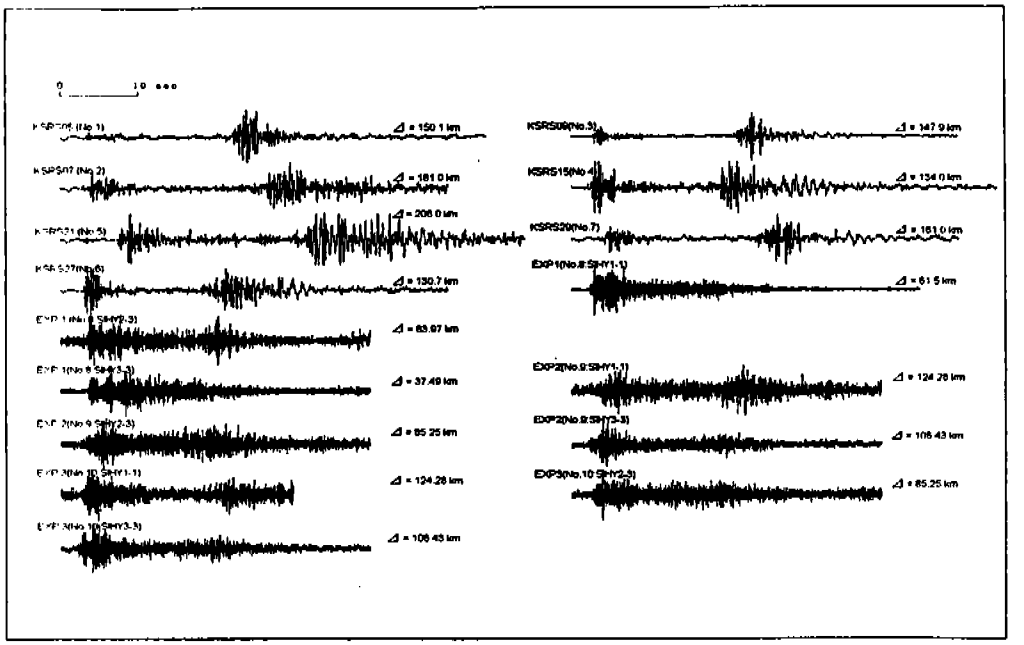

Figure 2. Seismograms of explosions used in this study. "No." indicate event number in the Table 2.

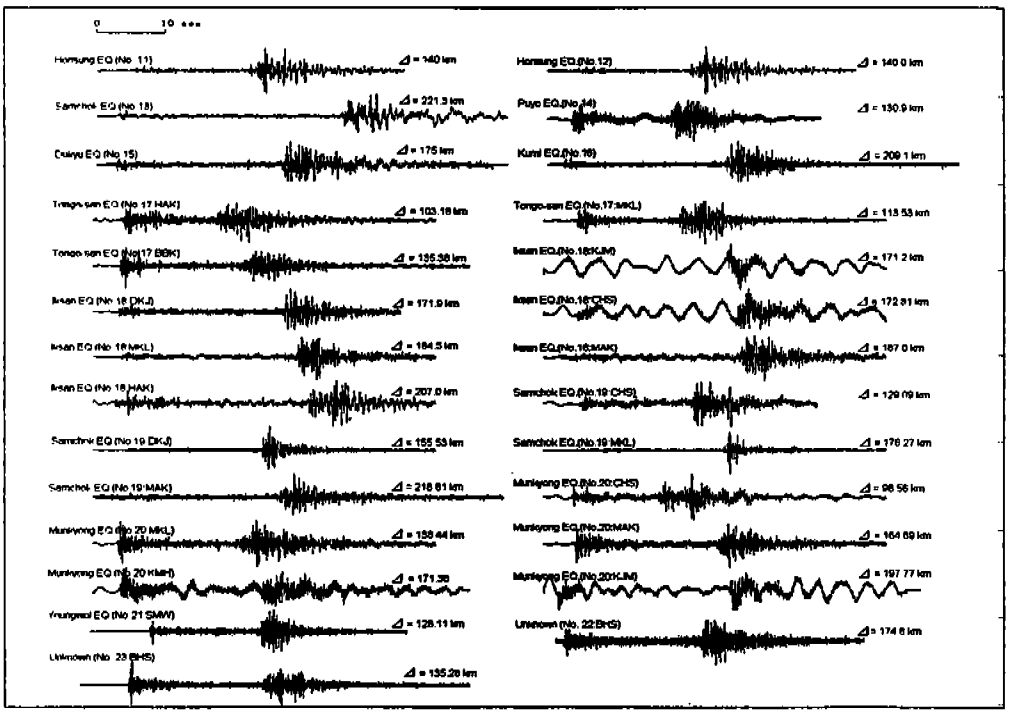

Figure 3. Seismograms of microearthquakes used in this study.

transform (or spectrum), and assumed a constant time delay δ_t between each shot or set of simultaneous shots(e. g., a row of shots), then the signal s(t) from the ripple-fired blast is the sum of all N shots :

$$s(t) = \sum_{m=0}^{N-1} r(m\delta_t)\, u(t - m\delta_t), \qquad (4)$$

where $r(m\delta_t)$ represents the number of charges at time $m\delta_t$ from the initiation of the blast. If time delays between shots are not uniform, the above equation is represented as a continuous integral :

$$s(t) = \int_{\tau=0}^{t_N} r(\tau)\, u(t-\tau)\, d\tau, \qquad (5)$$

where t_N is the total duration of the blast and $r(\tau)$ describes either the number of charges exploding at a specific time τ or the total size of the charges initiated at time τ. These equations represent the discrete convolution of two functions, the source function $u(t)$ for a single shot or row and the delay-time function $r(t)$ for the shooting pattern :

$$s(t) = r(t) * u(t). \qquad (6)$$

The Fourier transforms is

$$S(f) = R(f) \cdot U(f). \qquad (7)$$

If each of shots is equal size in similar conditions,

$$U(f) = \sum_{k=1}^{N} e^{-i2\pi f_k} \qquad (8)$$

Using the above equations, the amplitude spectrum of U(f) becomes (Gitterman and Torild, 1993) :

$$|U(f)| = \left| \frac{\sin(N\pi f \Delta t)}{\sin(\pi f \Delta t)} \right| \qquad (9)$$

Thus ripple-firing procedure can be assumed as a complex filter modulating the spectrum of single shot, so to speak some frequencies are enhanced and others are suppressed. Figure 4 shows feature of spectrum modulation that is proportional to the number of rows N. In this figure, we find absolute maxima at frequencies $f_{max} = k/\Delta t$ for k = 0, 1, 2, ···, minor maxima at frequencies $f_{mm} = (2k+1)/(2N\Delta t)$ for k = 1, 2, ···, N-2, N+2, ··· and minima or zeros at frequencies $f_{min} = k/(N\Delta t)$ for k = 1, 2, ···, N-1, N+1, ···. These principles allow us to predict the spectral modulations introduced by ripple firing known blast patterns(Smith, 1989, Gitterman et al., 1992). Spectral modulation due to ripple-fired explosions make diferent Pg/Lg ratios in the frequency domain because some frequencies are enhanced.

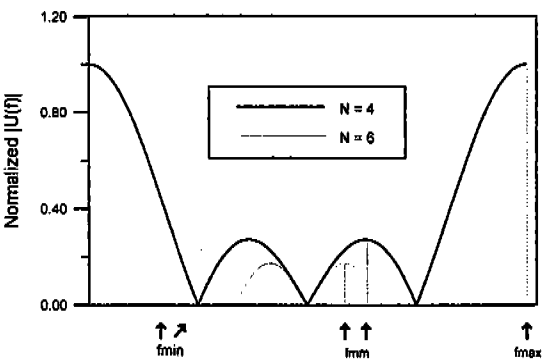

Figure 4. Normalized spectral characteristic of linear system for N=4 and N=6. The frequency of minima(fmin), maxima (fmax), and minor maxima)(fmm) depending on time delay and number of raw(shots).

Example spectrograms for the blast show that there are weak but clear spectrum modulation

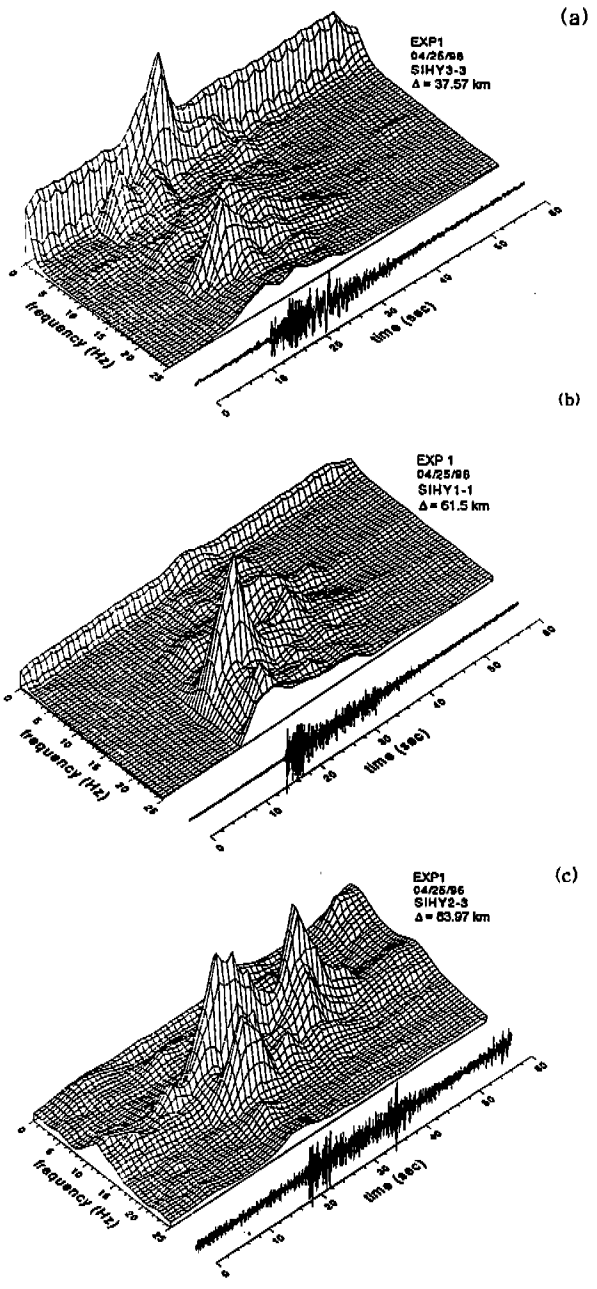

Figure 5. Spectrograms from quarry blast on 4/25/96 recorded at SIHY temporal seismic array(Event No. 8 in table 2).

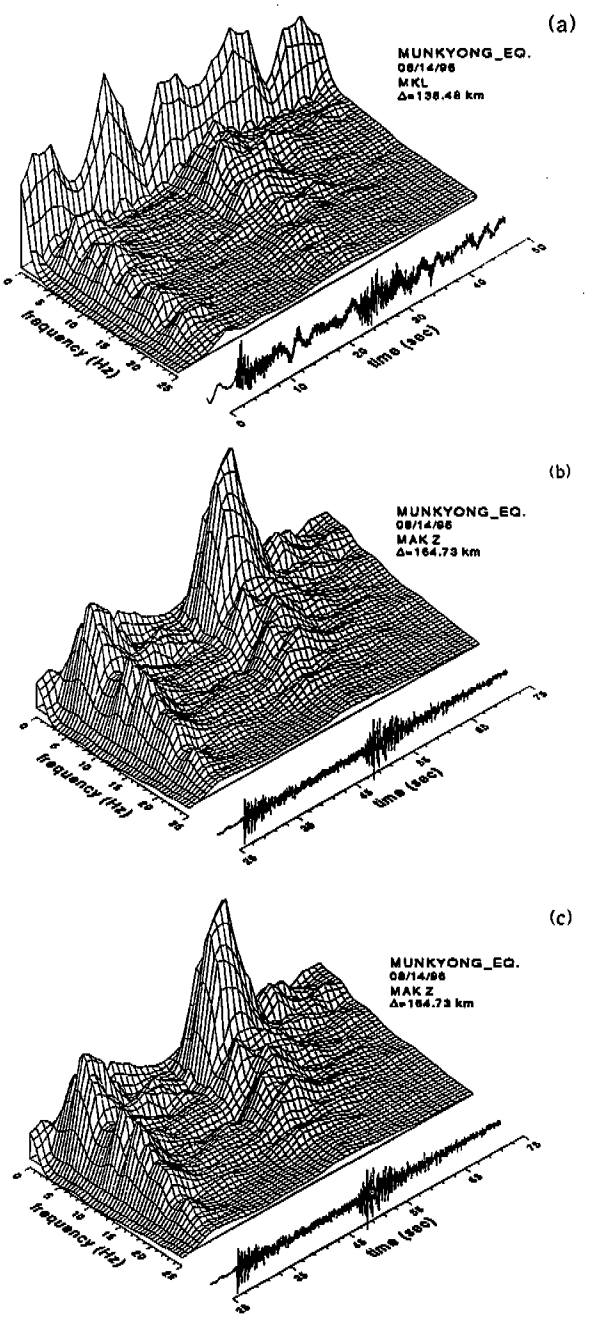

Figure 6. Spectrograms from Munkyong earthquake on 08/14/96 recorded at KIGAM seismic array(Event No. 21 in table 2).

and we can notice that body waves form quarry blasts have high energy and narrow frequency content above 10 Hz due to spectral modulation caused by ripple-firing of subshots independent of distance. The short-period Rg waves are essentially confined to depths of about 1 to 5 km and as such Rg signals are significant attenuation resulting from low Q materials in the shallow crust(Kim and Richards, 1996). Hence, Rg phases are observed only at near distance

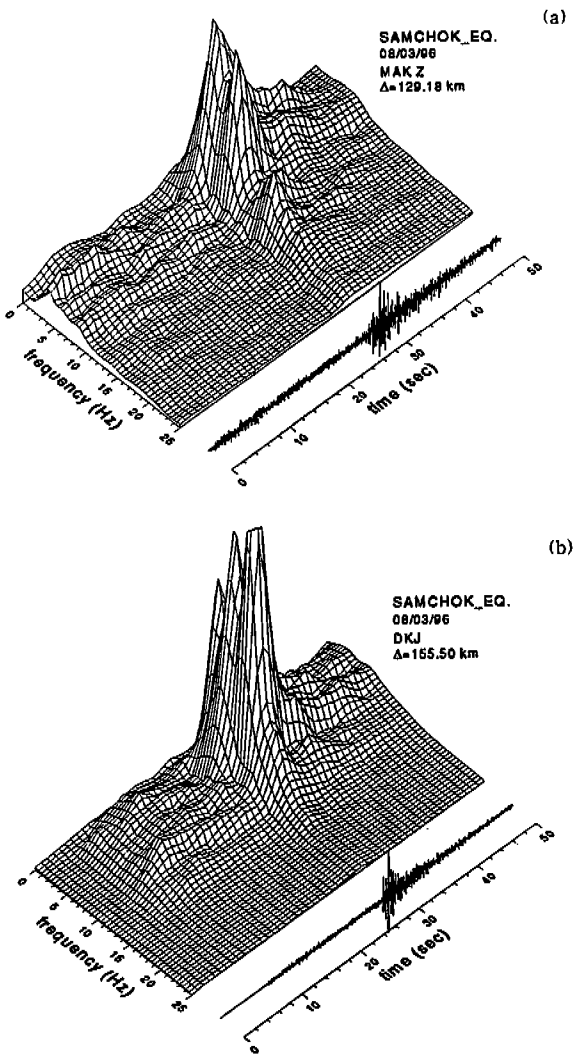

Figure 7. Spectrograms from Samchok earthquake on 8/3/96 recorded at KIGAM seismic array (Event No. 19 in Table 2).

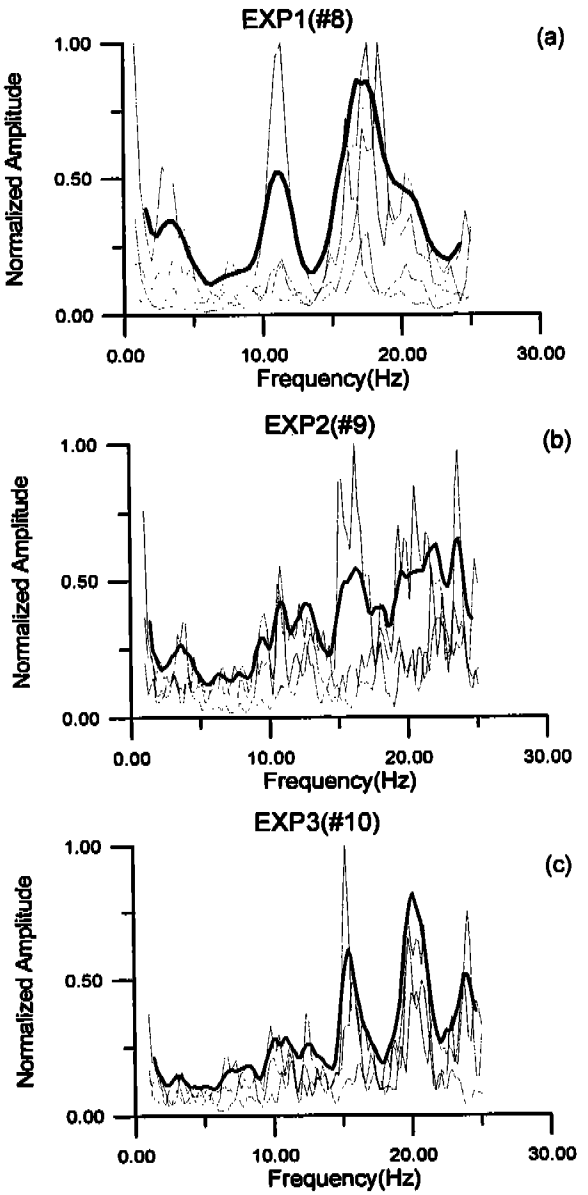

Figure 8. Summed spectra at three stations of quarry blasts. Dot lines indicate amplitude spectra of each station and thick lines indicate summed spectra.

ranges(Figure 5-a). S waves from earthquakes are stronger than P waves below a low 10 Hz, and microearthquakes have lower(below 10 Hz) dominant and more broad frequency content (Figure 5 and 7). Figure 8 shows summed amplitude spectra of P waves at three stations in the distance range 37 to 61 km(Fig 8-a) and 85 to 124 km(Fig. 8-b and 8-c) from quarry blasts and figure 8 is from earthquakes at three stations(Fig. 9-a), four stations(Fig. 9-b) and five stations(Fig. 9-c). Dot lines indicate spectrum of each stations and thick lines indicate their mean spectra. We can notice clear difference in P-wave amplitudes frequency content and above 10 Hz. The figure 8 shows spectra modulations over all quarry blasts and spectra of P wave from earthquakes have large amplitude in low frequency band(below 10 Hz) as well as high frequency band.

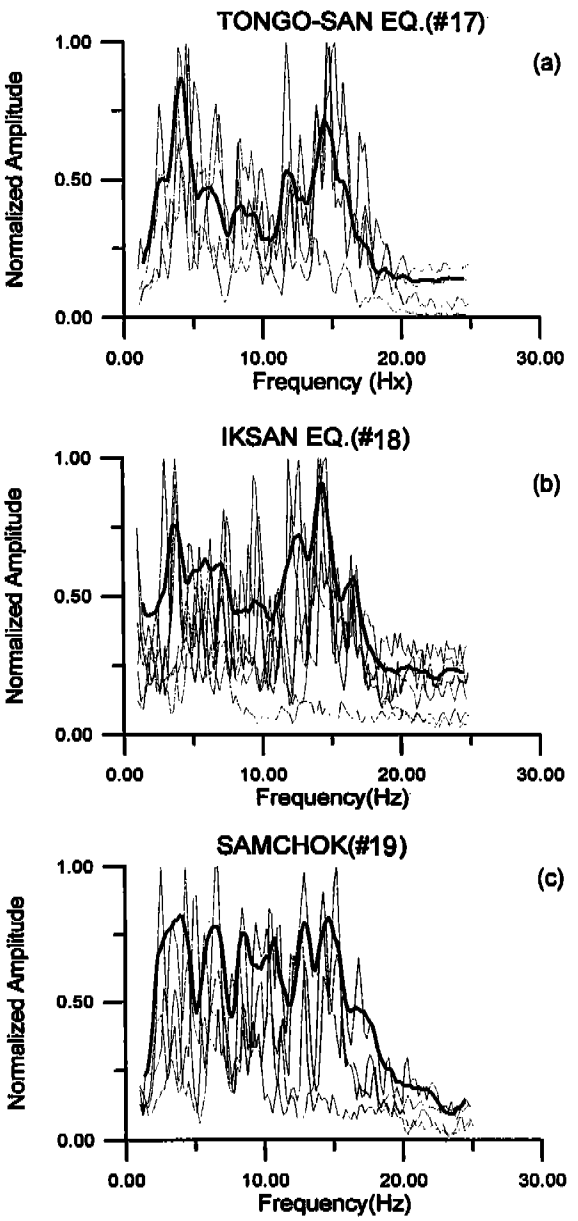

Figure 9. Summed spectra at four or five stations of earthquakes. Dot lines indicate amplitude spectra of each station and thick lines indicate summed spectra.

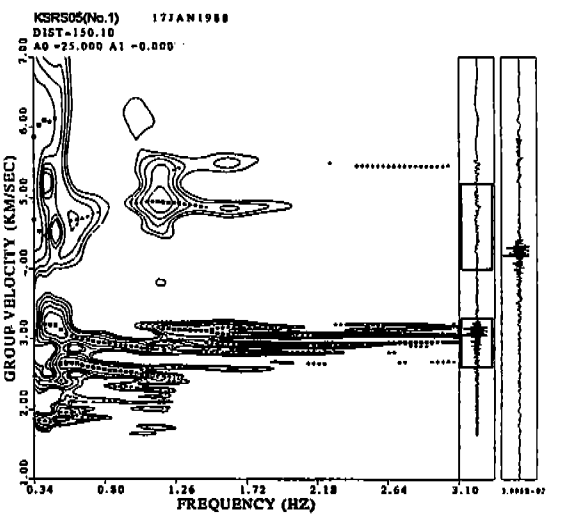

Figure 10. Group velocity of KSRS05(Event #1) is computed by the Multiple Filter Analysis(MFA). The largest amplitudes of envelope for each frequency are plotted as squares, then circles, triangles, and pulses for correspondingly smaller amplitudes. And the seismogram on the right is the waveform, while the inner trace represents the waveform scaled linearly versus apparent group velocity.

The Removal of Free Surface Interactions from Three-component Data

The key to the successful discrimination of various types of seismic sources is the clear observation of the signals radiated from the seismic sources. one of the most important problems is correction of the effects of the source to receiver paths on the observed regional signals(Kennett, 1991; Kim and Richards, 1996). Any theoretical description of the passage of seismic waves from source to receiver has to include the effects of the structure near the receiver. The presence of the free surface on which traction vanishes leads to reflection of upgoing waves back into the medium when they may undergo further interactions before return to the surface. In order to remove free surface effects, we rotate the components in the horizontal plane into a (Z, R, T) coordinate system radial and tangential to the path from the source using the azimuth. In the rotated coordinate system, using the notation of Aki and Richards (1980, chapter 5), the motion of the free surface itself is

$$\frac{P(t)\left[\frac{4\alpha p}{\beta^2}\frac{\cos i}{\alpha}\frac{\cos j}{\beta}, 0, \frac{-2\alpha}{\beta^2}\left(\frac{1}{\beta^2}-2p^2\right)\right]}{\left(\frac{1}{\beta^2}-2p^2\right)^2+4p^2\frac{\cos i}{\alpha}\frac{\cos j}{\beta}} = [\,R(t), 0, -Z(t)] \quad (10)$$

where α=surface P-wave velocity, β = surface S-wave velocity, i = angle of incidence of P-wave, j = angle of incidence of S-wave, p = slowness and sin i/α = sinj/β = p. Figure 11 shows theoretical sketch of ground motions(Kim and Richards, 1996) in a homogeneous half-space for a P-wave incident on a free surface with unit amplitude and an angle of incidence i ≈ 33.70° (= 0.1 s/km), surface P and S velocities : α= 5.5 km/s and β=3.1 km/s, respectively. The total ground motion of the free surface (shaded line) is shown above the surface level z = 0 and has amplitude 2.03 times the incident wave with an apparent angle of incidence i' = 36.12° . The motion of the incident P- and SV-wave can then be recovered as a linear combination of the radial, R(t), and vertical, Z(t), components available from three-component records. Thus above equation can be used to show that

$$P(t) = \frac{\cos 2j}{2\cos i}\cdot Z(t) + \frac{\beta}{\alpha}\sin j \cdot R(t) \quad (11)$$

$$SV(t) = \frac{\cos 2j}{2\cos j}\cdot R(t) - \sin j \cdot Z(t) \quad (12)$$

The estimate of the incident SH-wavefield is simply one half of the tangential component after rotation and is thus quite sensitive to the

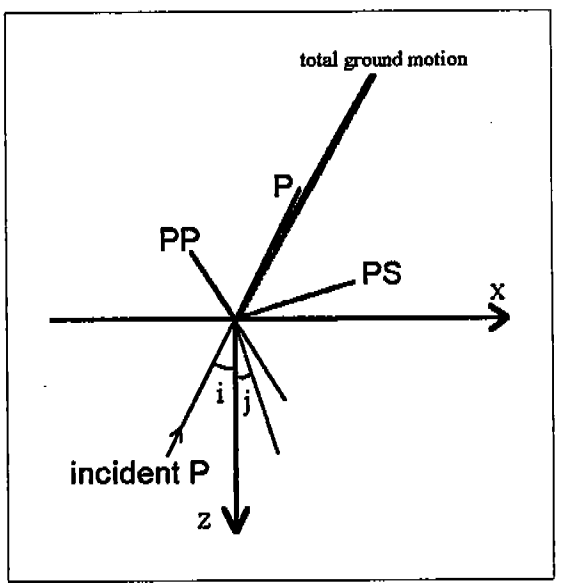

Figure 11. Theoretical sketch of ground motions in a homogeneous half-space.

azimuth employed(Kennett, 1991).

$$SH(t) = \frac{1}{2}\, T(t) \qquad (13)$$

Figures 12 and 13 show examples of free surface correction data. After correction of free surface effect, P waves are mainly on the P-wavevector component, and Lg waves are dominantly on the SV-wavevector component in case of explosions (see Figure 13).

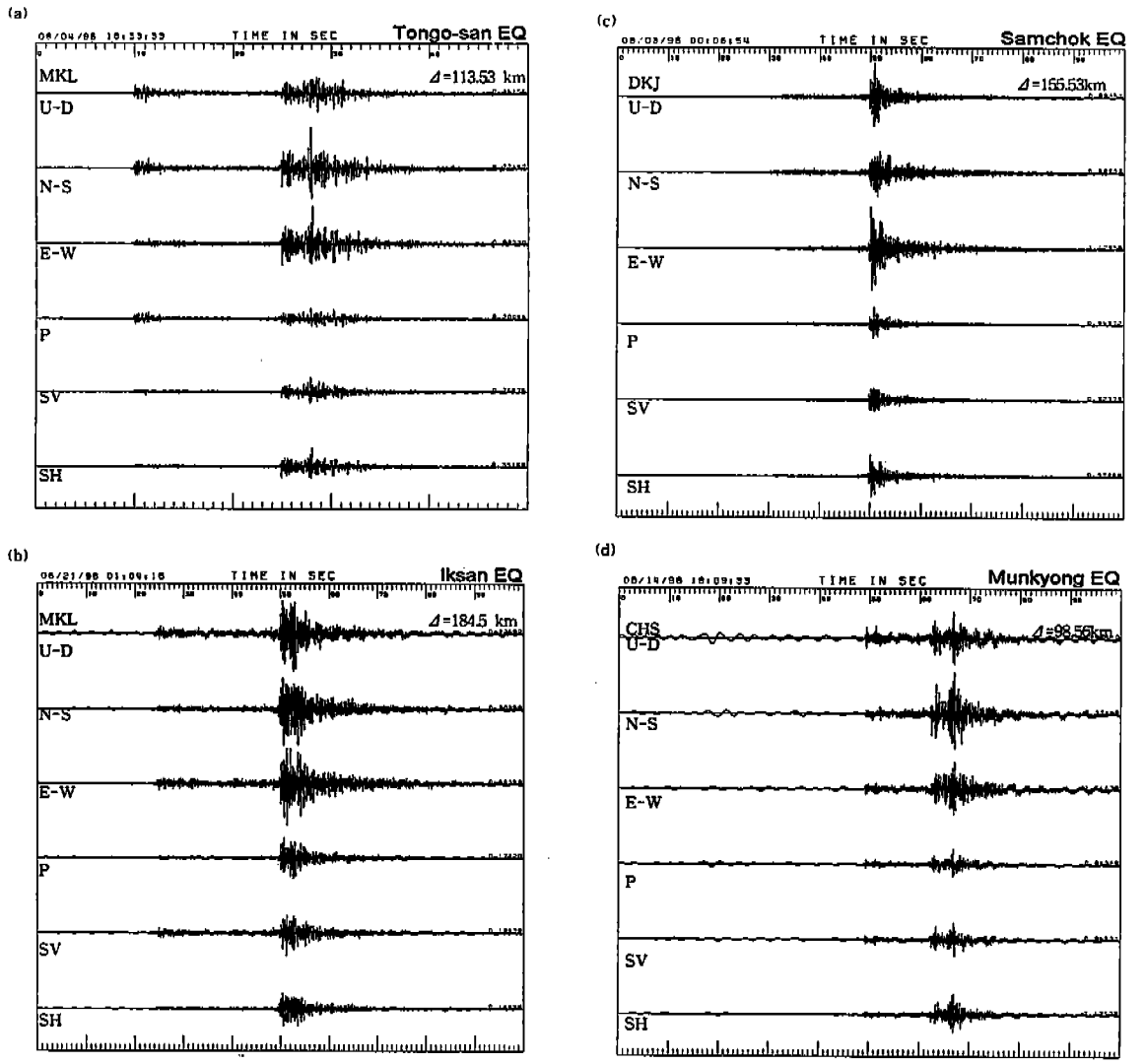

Figure 12. Example of free surface correction data. (Upper three traces) Row three-component records from Tongo- san earthquake(event no. 18). (Lower three trace) composite incident wavevector component traces(P, SV and SH) produced by applying free surface correction.

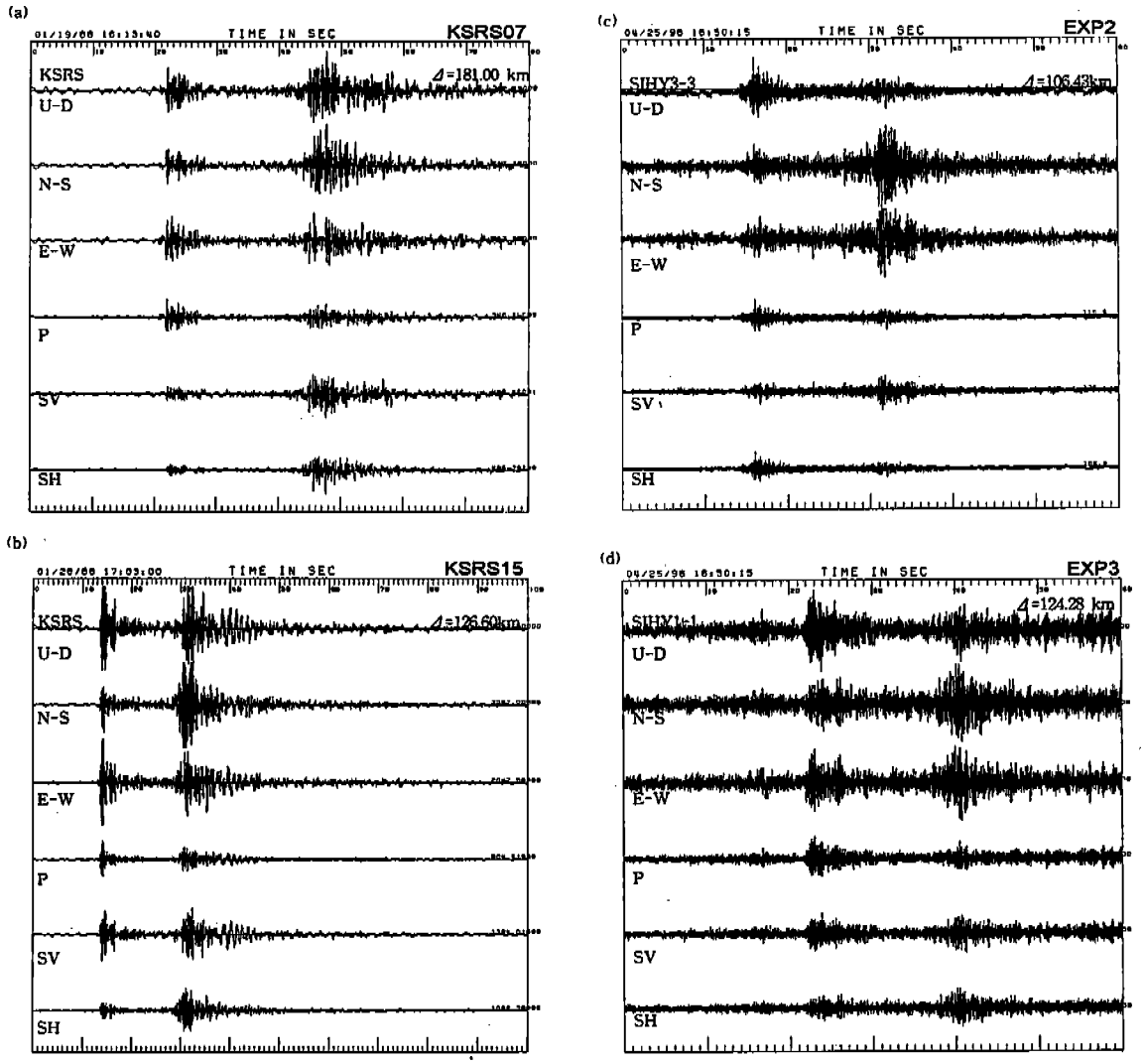

Figure 13. Example of free surface correction data. (Upper three traces) Row three-component records from quarry blast(event no. 8). (Lower three traces) composite incident wavevector component traces(P, SV and SH) produced by applying free surface correction.

Calculation of Pg/Lg Spectral Ratios

We calculated Pg/Lg ratios of all data(23 events in the table 2) below 10 Hz in order to use data recorded by KSRS and IRIS broad-band seismic stations with 20 SPS. To calculate Pg/Lg ratios, we removed free surface effects on our data since this procedure can make direct comparison between the P-, SV- and SH-wave amplitudes in a particular group velocity window and so get closer to the radiation characteristics from the source, especially with regard to the ratio of SV to SH in the regional

S-waves(Kennett, 1991). And the Pg/Lg ratios from the free surface corrected P-, SV- and SH-seismograms of three-component regional records are calculated from the average of the seven frequency bands : 0.5 to 3, 2 to 4, 3 to 5, 4 to 6, 5 to 7, 6 to 8 and 8 to 10 Hz and obtained for each station by defining

$$\frac{Pg}{Lg} = \frac{average(Pg_P)}{\sqrt{average(Lg_{SV})^2 + average(Lg_{SH})^2}} \quad (14)$$

where Pg_p = spectral amplitude of Pg-wave on the P-seismogram, Lg_{SV} = spectral amplitude of the Lg-wave on the SV-seismogram and Lg_{SH} = spectral amplitude of the Lg-wave on the SH-seismogram. Figure 14 shows result of

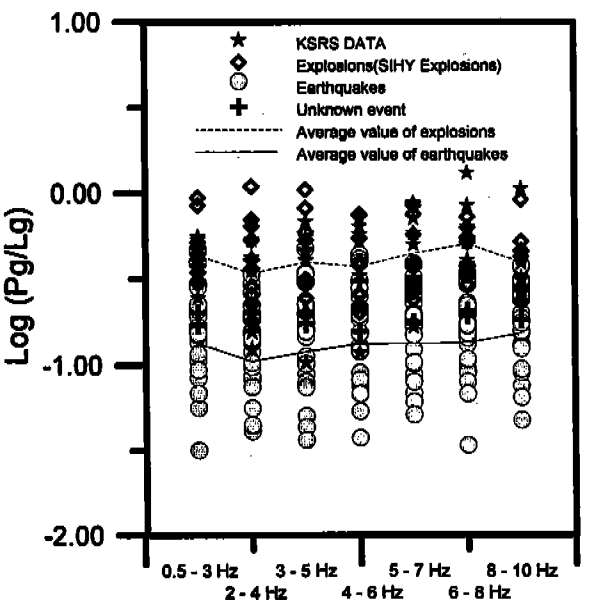

Figure 14. Pg/Lg ratios for the seven frequency bands. Dash lines show average values of explosions, and thin lines show average values of microearthquakes. Stars and diamonds represent KSRS data and explosions, respectively, and shaded circles represent microearthquakes. Thick crosses represent unknown events.

Log(Pg/Lg) ratios over seven frequency band. In this figure we can see the best separation is observed in 6 to 8 Hz. And with this result we can presume that the unknown events(event no. 23 and 24) are earthquakes.

Discussion and Conclusions

Through spectra analysis, it is found that the features of S waves from earthquakes are stronger than those of P waves over a broad frequency band(up to 20 Hz). P and S waves from earthquakes show that high spectral amplitudes appear in lower-frequency content (between 1 and 10 Hz; Figs 7 to 9), while P and S waves from quarry blasts have high amplitude in the part of high frequency(above 10 Hz) because of spectral modulation caused by ripple firing subshots. It is shown in the spectrograms and the summed spectra that the spectral modulation of ripple-fired blast is independent of paths and station site responses(Figs. 5 and 8).

We tried to calculate Pg/Lg ratios after correction of free surface effect for the sake of discrimination. A very useful product of this procedure is that we can make direct comparison between the P-, SV- and SH-wave amplitudes and so get closer to the radiation characteristics from source. On the SH vector component Lg waves have relatively small amplitude in case of explosions. This is of potential significance for discriminating different types of sources. After correction of free surface effect we calculate Pg/Lg ratios over seven frequency bands. And we obtain the best separation in 6 to 8 Hz band. The difference of the explosion Pg/Lg ratio with frequency is not totally understood. But one effect that could account for this is Rg to S (and Lg) scattering(Gupta et al., 1992; Steven, 1996) that would boost the Lg amplitudes at low frequencies.

A key to the Pg/Lg spectral ratio is the correction of regional signals for their source to receiver path effects and the frequency contents of P and S waves depend on specific propagation paths and local structure. So we have to carry out special study, for example the dispersive properties of surface waves.

Acknowledgment

This study was supported by the Korean Ministry of Education (BSRI-96-5420) and the Korean Research Foundation (96). This research was also partly financed by the Korea Institute of Geology, Mining and Materials (KIGAM).

Reference

Aki K. and Richards P. G., 1980, Quantitative Seismology, 2 vols, W. H. Freeman, San Francisco.

Alvert T. Smith, 1989, High-frequency seismic observations and models of chemical explosions : implications for the discrimination of ripple-fired mining blasts, Bull. Seism. Soc. Am., Vol. 79, No. 4, 1089-1110.

Chapman, M, C., Bollinger G. A., and Sibol M. S., 1992, Modeling delay-fired explosion spectra at regional distances, Bull. Seism. Soc. Am., Vol. 82, No. 6, 2430-2447.

Douglas R. Bqumgardt and Kathleen A. Ziegler, 1988, Spectral evidence for source multiplicity in explosions : application to regional discrimination of earthquakes and explosions, Bull. Seism. Soc. Am., Vol. 78, No. 5, 1773-1795.

Gupta, I. N., Chan W. W., and Wagner R. A., 1992, A comparison of regional phases from underground nuclear explosions at East Kazakh and Nevada Test Sites, Bull. Seism. Soc. Am. Vol. 82, 352-382.

Kennett B. L. N., 1991, The removal of free surface interactions from the three-component seismograms, Geophys. J. Int., 104, 153-163.

Kim So Gu and Park Yong-cheol, 1996, Discriminate between Small Explosions in Quarry Sites and Microearthquakes using amplitude ratio, Bull. Seism. Assoc. of the Far East (SAFE), Vol. 2, No. 1, 47-63.

Kim So Gu, Lee Seoung-Kyu, Mah Sang-Yun, and Park Yong-cheol, 1995, Detection and analysis of the artificial underground explosions in N. Korea using KSRS data, J. of Eng. Geology, Vol. 5, No. 2, 181-192.

Kim So Gu and Wu Zhongliang, 1996, Seismological problems associated with decoupled explosions : an overview, report of Science and Technology Policy Institute of Korea.

Kim W. Y., Simpson D. W., and Richards P. G., 1994, High-frequency spectra of regional phases from earthquakes and chemical explosions, Bull. Seism. Soc. Am., Vol. 84, No. 5, 1365-1386.

Kim W. Y. and Richards P. G., 1996, Discrimination of regional earthquakes and explosions using three-component high-frequency digital data, Modern Seismology-Proceedings of The Korea-China International Joint Seminar and Seismological Workshop edited by S. G. Kim, 46-61.

Taylor Steven R., 1996, Analysis of high-frequency Pg/Lg ratios from NTS explosions and Western U.S. Earthquakes, Bull. Seism. Soc. Am. Vol. 86, No. 4, 1042-1053.

Gitterman Yefim and Torild Van Eck, 1993, Spectra of Quarry Blasts and Microearthquakes Recorded at Local Distances in Israel, Bull. Seism. Soc. Am. Vol. 83, No. 6, 1799-1812.

김소구, 박용철
경기도 안산시 사1동 1271
한양대학교 지진연구소
TEL : 0345) 400-5532
FAX : 0345) 400-5830
e-mail : Sogukim @ hyung2.hanyang.ac.kr